scientific reports

Check for updates

OPEN

Dermal papilla cells-conditioned medium attenuates oxidative stress-induced senescence via ferroptosis inhibition

Zha Ru[1,2], Yu Wu[2], Qian Qu[1], Yong Miao[1], Lei Zhu[2]✉ & Zhiqi Hu[1]✉

Skin photoaging results primarily from chronic ultraviolet (UV) exposure, which disrupts dermal homeostasis and promotes cellular senescence. Dermal papilla cell-conditioned medium (DPC-CM) has emerged as a promising cell-free approach for skin rejuvenation. This study aimed to explore the anti-photoaging effects of DPC-CM and its potential regulation of ferroptosis. Mouse dermal papilla cells and skin fibroblasts were isolated and characterized. A photoaging model was established using UVA-irradiated fibroblasts, followed by treatment with DPC-CM at two concentrations, the ferroptosis inhibitor ferrostatin-1 (FER-1), or retinoic acid. UVA exposure led to reduced cell viability, impaired migration, increased senescence, elevated iron and reactive oxygen species levels, decreased glutathione, and altered expression of ferroptosis-related markers including nuclear factor erythroid 2-related factor 2 (NRF2), glutathione peroxidase 4 (GPX4), and solute carrier family 7 member 11 (SLC7A11). These changes were partially reversed by DPC-CM and FER-1. Proteomic analysis revealed that proteins in both dermal papilla cells and DPC-CM are associated with ferroptosis pathways. In vivo, DPC-CM significantly attenuated UVA-induced dermal aging. Collectively, these findings demonstrate that DPC-CM protects against photoaging by modulating ferroptosis, supporting its therapeutic potential in oxidative stress-related skin disorders.

Keywords Dermal papilla cells, Conditioned medium, Skin fibroblasts, Ferroptosis, UVA, Photoaging

Photoaging, a major form of exogenous skin aging, is primarily caused by ultraviolet (UV) radiation. It is characterized by rough, dry skin and a significant reduction in dermal collagen[1]. Ultraviolet A (UVA) radiation, the most prevalent component of the sun's UV spectrum, penetrates the skin and induces profound changes in connective tissue[2]. Excessive and repeated UVA exposure leads to oxidative stress, DNA damage, inflammation, and the degeneration of collagen and elastin, ultimately resulting in UVA-induced photoaging[3]. Despite these findings, no effective drugs have been developed to combat this condition. Therefore, it is crucial to deepen our understanding of the mechanisms underlying UVA-induced photoaging and to explore novel targeted therapies.

Ferroptosis is a form of iron-dependent, non-apoptotic cell death[4], which can participate in the pathological process of multiple diseases[5–7]. Ferroptosis is also characterized by lipid peroxidation, and this process is tightly regulated by the balance between oxidation and antioxidant systems within cells[8]. Ferroptosis inducers can alter glutathione (GSH) peroxidase activity through various mechanisms, leading to reduced antioxidant capacity, the accumulation of lipid reactive oxygen species (ROS), and, ultimately, oxidative cell death[9]. Recent studies have suggested that ultraviolet B (UVB)-induced skin photoaging is associated with ferroptosis, and inhibiting ferroptosis may mitigate skin aging[10]. For instance, Se-Met@GelMA hydrogel has been shown to reduce inflammatory responses, extracellular matrix remodeling, and ferroptosis in UV-exposed mice[11]. Additionally, methoxy-monobenzoylmethane, which acts through retinoic acid (RA) receptors, exhibits anti-aging effects by downregulating pro-inflammatory genes and reducing ferritin levels in skin tissues[12].

Although UVB is often associated with skin photoaging due to its ability to induce DNA damage and cause sunburn, UVA contributes more significantly to long-term structural changes in the skin, primarily through oxidative stress and collagen degradation. While UVB induces more immediate effects like erythema and DNA damage, UVA's effects are deeper and more chronic. Both UVA and UVB promote oxidative stress and

[1]Department of Plastic and Aesthetic Surgery, Nanfang Hospital of Southern Medical University, No 1838, Guangzhou North Road, Guangzhou 510515, China. [2]Department of Dermatology and Aesthetic Surgery, The Third Affiliated Hospital of Sun Yat-Sen University, No 600, Tianhe Road, Guangzhou 510630, China. ✉email: zhulei@mail.sysu.edu.cn; huzhiqidr163@i.smu.edu.cn

inflammation, but UVA-induced photoaging involves more persistent dermal changes. Given these differences, our study aimed to investigate how ferroptosis contributes to UVA-induced photoaging. Specifically, we explored the potential of dermal papilla cell-conditioned medium (DPC-CM) to regulate ferroptosis and reduce skin aging caused by UVA exposure.

Stem cell therapy is increasingly being utilized as a treatment across various fields and is gaining traction in dermatology[13]. Studies have shown that stem cells repair aging skin tissue by secreting cytokines, growth factors, and proteins, thereby achieving skin rejuvenation[14,15]. The dermal papilla (DP), identified as the niche for hair follicle mesenchymal stem cells, plays a crucial role in tissue regeneration and in vitro reprogramming, including the regulation of hair growth[16,17]. DP cells act as signaling centers within hair follicles, regulating hair formation and cycling through paracrine secretion[18]. These cells are also essential for the development, growth, and regeneration of hair follicles[19]. Additionally, previous study demonstrated that DP cells contribute to the early stages of new blood vessel formation in transplanted skin substitutes, accelerate the maturation of vascular networks in nude mice, reduce inflammation, and facilitate the remodeling of the extracellular matrix[20].

Conditioned medium (CM) derived from cells is regarded as a rich source of paracrine factors, including exosomes and cytokines. Adding CM to injured tissues has been shown to enhance metabolism, improve oxygen supply, reshape the extracellular matrix, promote stem cell migration, and prevent further organ damage[21]. Stem cell-derived CM is believed to exert anti-aging effects on the skin[22]. Research has further demonstrated that CM from adipose-derived stem cells can improve skin barrier function at both cellular and structural levels, enhance the activity of hair follicle stem cells by modulating transforming growth factor beta 2 (TGF-β2), and mitigate photoaging and extracellular matrix degradation associated with UV exposure[23]. However, the specific functions of DP cell-derived CM (DPC-CM) and its relationship with ferroptosis in UVA-induced photoaging remain unclear.

While DPC-CM shows great promise for skin rejuvenation and mitigating UVA-induced photoaging, challenges such as batch-to-batch variability in its composition may compromise the reproducibility and consistency of results. Our study further standardized the culture conditions and analyzed multiple DPC-CM batches to minimize variation and ensure data reliability. This strategy strengthens the credibility of our findings and supports the therapeutic potential of DPC-CM in photoaging treatment.

Building on this background, we hypothesize that DPC-CM plays a critical role in regulating ferroptosis during UVA-induced photoaging. In this study, we aim to investigate the mechanisms underlying the interaction between DPC-CM and ferroptosis through in vivo and in vitro experiments. Our findings could deepen the understanding of the molecular mechanisms by which DPC-CM regulates ferroptosis and pave the way for novel therapeutic strategies targeting photoaging.

Materials and methods

Ethics approval statement

All methods were conducted in accordance with relevant guidelines and regulations. Animal experiments were approved by the Guangzhou Forevergen Medical Laboratory Animal Center (Approval No. IACUC-AEWC-F231112027). Additionally, the studies adhered to the Animal Research: Reporting of In Vivo Experiments (ARRIVE) guidelines and the Institutional Animal Care and Use Committee (IACUC) Handbook (third edition).

Extraction of mouse DP cells and collection of DPC-CM

C57BL/6 mice in the growth phase were used for dermal papilla (DP) cell extraction. Before any procedures, mice were anesthetized using CO_2 to ensure humane treatment. The backs of the mice were shaved and depilated, followed by disinfection with 75% alcohol for 5 min. After disinfection, the skin was carefully clipped, and the dermal side was turned upwards. The murine membrane layer was gently separated using microscopic forceps, and the skin was rinsed 2–3 times with phosphate-buffered saline (PBS). The prepared skin was placed into a 6 cm Petri dish, and 3 mL of 0.2% collagenase was added for digestion. The dish was incubated at 37 °C for 1.5–2 h to allow proper digestion. After digestion, the skin was washed 3–5 times with PBS. The dermal side of the skin was turned upwards again, and the DP spheres were gently clipped or scraped off using microscopic scissors or a razor blade. The DP spheres were then gently suspended in PBS by pipetting them up and down for 5–10 min. Next, the DP spheres were isolated and purified using the Ficoll gradient centrifugation method. The single cells and impurities were separated from the DP spheres through different density gradient layers. Pure DP spheres were collected for further experiments. To obtain DPC-conditioned media (DPC-CM), cells were cultured in knockout DMEM (DMEM-KO, a medium suitable for the culture of embryonic stem (ES) cells, commonly used in combination with serum replacement (SR) for culturing mouse and human ES cells) medium and incubated until 80% confluence was reached. After 24 h, the conditioned media was collected into pre-chilled tubes, centrifuged at 310 g for 6 min at 4 °C, and filtered through 2 μm filters. The resulting media was collected in pre-chilled 1.5 mL microcentrifuge tubes for further use[24].

Extraction of mouse skin fibroblasts

For skin fibroblast extraction, C57BL/6 mice were anesthetized using CO_2 before any procedures. The dorsal skin was shaved and depilated and disinfected with 75% alcohol for 5 min. The depilated skin was clipped and placed in a 10 cm Petri dish containing PBS. After washing the skin 2–3 times with PBS, the skin was transferred to a 6 cm Petri dish (without any liquid). Using ophthalmic scissors and microscopic scissors, the skin was carefully cut into small pieces. Then, 3–5 mL of collagenase was added, and the dish was incubated at 37 °C for 1–1.5 h. During this incubation, individual cells were released from the tissue, as observed under a microscope. After digestion, PBS was added to neutralize the cells. The cell suspension was then filtered through a 70/40 μm mesh filter to remove any large debris. Following centrifugation at 1000 g for 5 min, the cells were resuspended

and seeded into a T25 culture flask with 2.5 mL of 20% conditioned culture medium. Fibroblasts adhered rapidly to the culture surface. To minimize contamination risk, the culture medium was replaced 1–2 days after the primary mouse skin fibroblasts were extracted, with 4 mL of 10% whole culture medium.

Euthanasia of mice

At the end of the experimental procedures, mice were euthanized using CO_2 at a rate of 50% of the volume displacement per min (VDR/min), following ethical standards for animal research. This method ensures the humane euthanasia of the animals, minimizing distress and pain.

Immunofluorescence (IF)

IF was performed to measure the expression of mouse DP cell markers alkaline phosphatase (ALP), cluster of differentiation 133 (CD133), and neural cell adhesion molecule (NCAM), as well as mouse skin fibroblast markers α-SMA and Vimentin. The cells were fixed using pre-chilled 4% paraformaldehyde (in PBS) either at 4 °C for 40 min or for 10 min. After fixation, paraformaldehyde was removed at room temperature, followed by two washes with 0.1% Triton X-100 solution (in PBS) for 5 min each. Subsequently, the cells were blocked with 3% blocking serum (in PBS) for 1 h. The primary antibodies-ALP (11,187–1-AP, Proteintech), CD133 (66,666–1-Ig, Proteintech), NCAM (14,255–1-AP, Proteintech), α-SMA (14,395–1-AP, Proteintech), and Vimentin (22031-1-AP, Proteintech)-were incubated with the cells at 4 °C overnight. After the overnight incubation, the samples were rewarmed to room temperature for 45 min. Fluorescently labeled secondary antibodies were then applied and incubated for 1 h, ensuring protection from light throughout the process. Nuclear staining was performed with DAPI dye. A 50 µL solution per well was applied and incubated away from light for 10 min. Finally, the cells were sealed with mounting medium, allowed to solidify, and photographed. All IF staining experiments were performed in three independent biological replicates.

Cell treatment

UVA treatment of mouse skin fibroblasts was used to construct a cell photoaging model. To investigate the mechanism of ferroptosis in DP cells during cell senescence, skin fibroblasts were treated with the ferroptosis inhibitor ferrostatin-1 (FER-1, HY-100579, MCE). The groups included the Negative control (NC) group, consisting of normal cultured mouse skin fibroblasts; UVA group, where fibroblasts were irradiated with 6 J/m^2 UVA and cultured in normal medium for 24 h; and UVA + FER-1 group, where fibroblasts were treated with 2 µM FER-1, irradiated with 6 J/m^2 UVA, and cultured in normal medium for 24 h. The UVA irradiation was performed using a UVA-340 nm ultraviolet aging test lamp (Yixian UVA-340 T5 6W). Cells were placed at a distance of 10 cm from the lamp and irradiated for 2 h, receiving a total UVA dose of 6 J/cm^2[25]. After irradiation, cells were cultured for an additional 48 h. Additionally, fibroblasts were treated with UVA and exposed to a concentration gradient of DPC-conditioned medium (DPC-CM). The groups were as follows: NC group, UVA group, UVA + low group (where fibroblasts were treated with 30% DPC-CM, irradiated with 6 J/m^2 UVA, and cultured in normal medium for 24 h), UVA + high group (where fibroblasts were treated with 90% DPC-CM, irradiated with 6 J/m^2 UVA, and cultured in normal medium for 24 h), and UVA + RA group (where fibroblasts were treated with 200 nM RA, irradiated with 6 J/m^2 UVA, and cultured in normal medium for 24 h). The concentrations of 30% and 90% DPC-CM were chosen with reference to commonly used ranges for conditioned media[26]. In our experiments, these two concentrations produced distinct effects on cell viability and cellular senescence, making them appropriate for representing low and high treatment levels. Each treatment group was analyzed in three independent experiments to ensure data reproducibility and consistency.

Mass spectrometry

Total protein was extracted from mouse DP cells and DPC-CM, and the common proteins were analyzed using mass spectrometry. Protein extraction was performed using the buffer (4% SDS, 100 mM Tris/HCl pH 7.6, 0.1 M DTT), followed by quantification with the BCA method. Equal amounts of protein from each sample were digested with trypsin, desalted using octadecylsilane (C18) cartridges, and lyophilized. The dried peptides were reconstituted in 0.1% formic acid solution, and their concentrations were determined by OD_{280}. Each sample was then subjected to high-performance liquid chromatography (HPLC) separation using buffer A (0.1% formic acid in water) and buffer B (0.1% formic acid in 84% acetonitrile). After column equilibration in 95% buffer A, peptides were loaded and separated on an analytical column. A Venn diagram was used to display the proteins identified in both DP cells and DPC-CM. In this study, Gene Ontology (GO) and Kyoto Encyclopedia of Genes and Genomes (KEGG) analyses were conducted using Database for Annotation, Visualization and Integrated Discovery (DAVID) version 6.8 (http://david.abcc.ncifcrf.gov)[27,28]. The top 20 GO terms or KEGG pathways with the most significant enrichment were selected for visualization. Additionally, the online database STRING was used to predict the presence or absence of protein interactions, and protein–protein interaction (PPI) networks were subsequently mapped. Protein extraction and mass spectrometry analysis were conducted in biological triplicates. Mass spectrometry was performed in positive ion mode using a high-resolution instrument. Common proteins were identified based on consistent detection across at least three independent samples.

Animals

Kunming mice (female, 20–25 g, 7–8 weeks old) were purchased from Huateng BioScience. Kunming mice were selected for this study based on their suitability for the photoaging model, as indicated in previous research[25], which supports their use in similar experimental setups. Before the experiment, the mice were acclimatized for 7 days with normal feeding and provided free access to food and water for the following 24 h. Then, the backs of the mice were shaved to an area of approximately 2 cm × 2 cm, with the skin left bare. The mice were

randomly divided into 4 groups: NC group, UVA group, UVA + CM group, and UVA + RA group, with 6 mice in each group. Anesthesia was performed on the mice using a multi-channel small animal anesthesia machine for inhalation anesthesia, with a ventilation rate of 1.5–2 L/min. The induction concentration was 4% isoflurane, and the maintenance concentration was 1.5% isoflurane. The mouse was considered to have reached a state of complete anesthesia when it was lying on its back with stable heartbeat and respiration, relaxed muscles, immobile limbs, absence of whisker tactile response, and loss of the pedal reflex. A photoaging model was established by irradiating the bare back skin of mice with preapplied 1% 8-methoxypsoralen (8-MOP) and UVA light. The irradiation was carried out using a UVA-340 nm ultraviolet aging test lamp (Yixian UVA-340 T12 40W). The mice were exposed at a distance of 10 cm from the lamp, with a total irradiation time of 16.29 h over 7 days, accumulating a total UVA dose of 95 J/cm^2. The UVA exposure was divided into daily sessions of 1.5–2 h, ensuring consistency. Except for the NC group, the skin of the other shaved mice was coated with 1% 8-MOP once a day for 1.5–2 h, followed by UVA irradiation. The radiation was performed at the same time each day to ensure consistency. The UVA output was measured using a calibrated radiometer to ensure accurate dose delivery. To prevent contamination with UVB, appropriate UV filters were placed over the mice during irradiation, allowing only UVA radiation to reach the skin. The photoaging model was successfully established when the skin on the back of the mice became dry, peeled, and in some cases developed local ulcers. Analgesia was administered with meloxicam (MCE, HY-B0261, 2 mg/kg/day) for 3 days. Subsequently, the UVA + CM group was coated with polyethylene glycol (PEG)@DPC-CM. The UVA + RA group was coated with PEG@RA. The NC and UVA groups were coated with PEG. Among them, 1% 8-MOP was prepared as follows: 100 g of PEG was weighed, 1 g of 8-MOP (HY-30151, MCE) was added, mixed well, and stored at 4 °C. PEG was prepared as follows: 200 g of PEG, average Mn 400 (P815616-250 g, Macklin), and average Mn 1500 (P815606-500 g, Macklin) were weighed, mixed well to form a substrate of 400 g, and stored at 4 °C. PEG@DP cell supernatant was prepared as follows: DP cells were cultured, 100 mL of CM were collected, subjected to differential centrifugation at 1000 g for 10 min and 10,000 g for another 10 min to remove cellular debris and large particles. The supernatant was then concentrated using a 100 kDa ultrafiltration device (e.g., Amicon Ultra), which retained exosomes and protein complexes while removing smaller molecules such as salts and free proteins. The volume was reduced to one-tenth of the original. The concentrated CM was then frozen at -80 °C, and then freeze-dried into 1 mL of concentrated CM. 100 g of PEG was weighed, mixed with 1 mL of concentrated CM, and stored at 4 °C. PEG@RA was prepared as follows: 100 g of PEG was weighed, 0.05 g of RA was added, mixed well, and stored at 4 °C for later use. The skin of the mice in each group was monitored after 10 days of continuous treatment. Mice were euthanized at a VDR/min rate of 50% using 100% CO_2, and samples were then collected.

Cell counting kit 8 (CCK-8) assay

The CCK-8 assay was utilized to assess the viability of mouse skin fibroblasts. For each experiment, 4000 cells were seeded per well in 96-well plates, and the cells were allowed to adhere for 24 h in a cell culture incubator (37 °C, 5% CO_2). Following this incubation, 100 µL of cell suspension was added to each well. After 48 h of cell attachment, 10 µL of CCK-8 solution (G4103, Servicebio) was added to each well. The cells were then incubated for an additional 2 h in the incubator. Absorbance at 450 nm was measured using a microplate reader. Each group was tested in six replicate wells per experiment, and the entire assay was independently repeated three times.

SA-β-galactosidase (Gal) staining

The Senescent Cell β-Gal Staining Kit (G1073, Servicebio) was used to assess the senescence of mouse skin fibroblasts. Skin fibroblasts were cultured, and the cell culture medium was aspirated. The cells were then washed twice with PBS. Next, 1 mL of β-Gal staining fixative was added, and the fibroblasts were fixed for 15 min. Following fixation, the fixative was discarded, and the cells were washed three times with PBS for 2 min each. Afterward, PBS was carefully aspirated using a pipette, and 1 mL of β-Gal staining working solution was added. The fibroblasts were incubated at 37 °C for 2 h or overnight. The cells were then observed under a light microscope, and the staining solution was removed once the positive cells were adequately colored. β-Gal staining was performed in three independent experiments with consistent conditions across replicates.

Detection of β-Gal activity

Approximately 0.1 g of mouse skin tissue was weighed, and 1 mL of extract was added for ice-bath homogenization. The homogenized sample was centrifuged at 15,000 × g and 4 °C for 10 min. The supernatant was collected and kept on ice. β-Gal activity in mouse skin was then measured according to the instructions provided with the β-Gal Activity Test Kit (BC2585, Solarbio). Measurements were performed using samples from three independently treated animals in each group.

Scratch assay

Cell migration was assessed using the scratch assay. Cells in the exponential growth phase were detached using trypsin (Thermo Fisher, Cat. No. 25300–054) and seeded into 6-well plates at a density of 1×10^6 cells per well. Once the cells adhered to the plate, the medium was replaced, and mitomycin C was added at the desired final concentration for 1 h to inhibit cell division. A 200 µL pipette tip (Thermo Fisher, Cat. No. 236203) was used to create scratches in the monolayer. After scratching, the detached cells were removed, and a fresh culture medium was added. The cells were then incubated for further culture. Images were taken at 0, 6, 24, and 48 h from 8 randomly selected scratch fields at each time point. Image-J software was used to measure the wound distance and calculate the migration rate. The migration rate was calculated using the formula: migration rate = (0 h—other time points) / 0 h. The scratch assay was independently performed three times to validate the reproducibility of cell migration patterns.

Biochemical detection

Iron, GSH, and ROS levels in mouse skin fibroblasts and tissues were measured using the following assay kits: Iron (A039-2-1, Nanjing Jiancheng Bioengineering Institute), GSH (A006-2-1, Nanjing Jiancheng Bioengineering Institute), and ROS (BL714A, Biosharp). Each biochemical assay (iron, GSH, ROS) was conducted in three biological replicates per group.

Western blot

The expressions of nuclear factor erythroid 2-related factor 2 (NRF2), glutathione peroxidase 4 (GPX4), and solute carrier family 7 member 11 (SLC7A11), as well as the expressions of Collagen I and alpha-smooth muscle actin (α-SMA), were analyzed by Western blot. Total protein was extracted using RIPA buffer (Radio-Immunoprecipitation Assay buffer) (R0010, Solarbio Life Science). Protein quantification was performed according to the BCA Protein Assay Kit (Bicinchoninic Acid Protein Assay Kit) (BL521A, Biosharp). The target proteins were separated by 15% polyacrylamide gel electrophoresis (SDS-PAGE) (Sodium Dodecyl Sulfate–Polyacrylamide Gel Electrophoresis) and then transferred to a PVDF (Polyvinylidene Fluoride) membrane (ISEQ00010, Merck Millipore). To block non-specific binding sites, the membrane was incubated with 5% bovine serum albumin (BSA) solution in Tris-buffered saline with Tween-20 (TBST) for 1 h at room temperature. The membrane was then incubated overnight at 4 °C with primary antibodies: NRF2 (16,396–1-AP, Proteintech), GPX4 (67,763–1-Ig, Proteintech), SLC7A11 (A13685, ABCLONAL), Collagen I (14,695–1-AP, Proteintech), α-SMA (14,395–1-AP, Proteintech), and β-actin (66,009–1-Ig, Proteintech). After incubation, the membrane was washed three times with TBST for 10 min each to remove unbound antibodies. The membrane was then incubated with the appropriate secondary antibody for 1–2 h. Finally, chemiluminescent detection (BL520A, Biosharp) was used, and the optical density of the target bands was analyzed using ImageJ software. β-actin was used as an internal control to compare the expression levels of the target proteins after different treatments. Western blot experiments were repeated three times independently using different sample preparations to ensure consistent results.

Hematoxylin–eosin (H&E) staining

H&E staining was used to examine pathological changes in the epidermis and dermis. Freshly extracted tissues were fixed, conventionally embedded in paraffin, and sectioned into slices 3–8 μm thick. Sections were deparaffinized twice in xylene for 5–10 min each, followed by rehydration through a series of ethanol gradients (100%, 95%, 85%, and 75%) for 3 min each. The sections were then placed in distilled water for 2 min before staining with hematoxylin solution (G1100, Solarbio) for 2–20 min. Excess stain was rinsed off with distilled water to remove residual dye. The sections were subsequently differentiated in a differentiation solution for 10–60 s, washed twice with tap water for 3–5 min each, and stained with eosin solution for 30 s to 2 min. Excess eosin was poured off, and the sections were rapidly dehydrated through a graded ethanol series (75%, 85%, 95%, and 100% ethanol [I]) for 2–3 s each. They were then rinsed in 100% ethanol (II) for 1 min, followed by two washes in xylene for 1 min each. Finally, the sections were mounted with neutral gum and observed under a microscope. Tissue samples from three randomly selected animals per group were used for H&E staining.

Masson staining

The Masson trichrome staining kit (G1340, Solarbio) was used to evaluate pathological changes in the epidermis and dermis. The sections were first deparaffinized to water, then stained with prepared Weigert's Iron Hematoxylin for 5–10 min. Sections were differentiated in an acidic ethanol solution for 5–15 s and washed with water. After rinsing in distilled water for 1 min, sections were treated with Masson's blue solution for 3–5 min, followed by staining with Lichun red solution for 5–10 min. A weak acid working solution was prepared by mixing distilled water and weak acid solution in a 2:1 ratio. Sections were washed in this solution for 1 min, treated with phosphomolybdic acid solution for 1–2 min, washed again in the weak acid solution for 1 min, and stained with aniline blue solution for 1–2 min. After another 1-min rinse in the weak acid solution, sections were rapidly dehydrated in 95% ethanol for 2–3 s, followed by three rounds of dehydration in anhydrous ethanol for 5–10 s each. Finally, sections were cleared in xylene three times for 1–2 min each and mounted with neutral gum. Masson staining was performed on skin tissues collected from three independent animals in each group.

Statistical analysis

All statistical analyses were performed using GraphPad Prism 8.0. Quantitative data are presented as means ± standard deviation (SD). Comparisons between two groups were made using Student's t-test, while one-way analysis of variance (ANOVA) was applied for comparisons among multiple groups. A P value of less than 0.05 was considered statistically significant. Each experiment was independently repeated at least three times to ensure reproducibility. Throughout the study, consistent experimental protocols, reagent sources, and exposure parameters were maintained to minimize inter-assay variability.

Results

Identification of primary mouse DP cells and skin fibroblasts

We first isolated and cultured mouse DP cells and skin fibroblasts. IF analysis was performed to detect the expression of mouse DP cell markers ALP, CD133, and NCAM, as well as skin fibroblast markers α-SMA and Vimentin. The results demonstrated positive staining for ALP, CD133, and NCAM in mouse DP cells (Fig. 1A) and positive staining for α-SMA and Vimentin in mouse skin fibroblasts (Fig. 1B). These findings confirm the successful isolation and identification of primary mouse DP cells and skin fibroblasts.

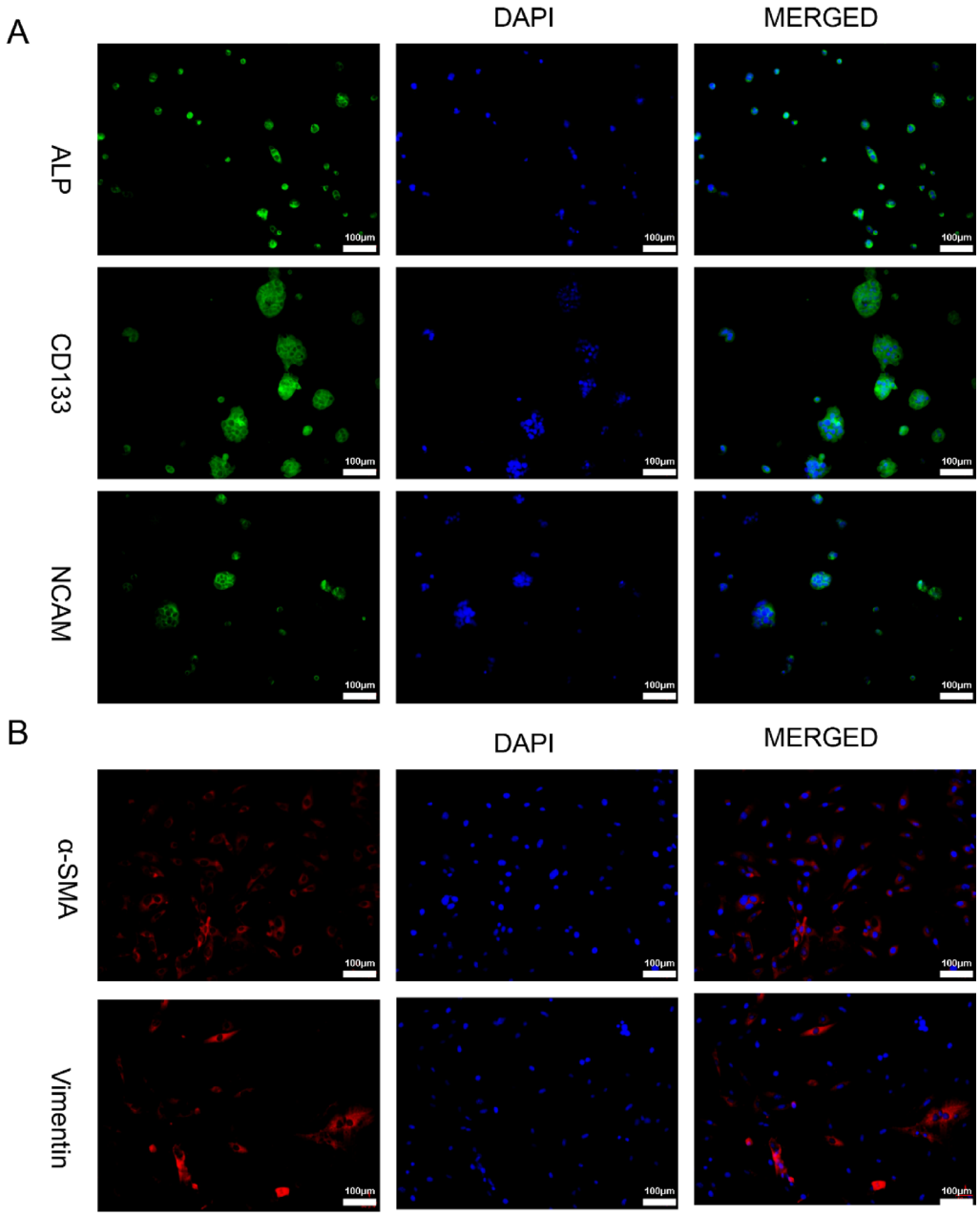

Fig. 1. Identification of primary mouse DP cells and skin fibroblasts. (**A**) IF staining of mouse DP cells markers ALP, CD133, and NCAM, scale bar = 100 μm. (**B**) IF staining of mouse skin fibroblasts markers α-SMA and Vimentin, scale bar = 100 μm.

UVA promoted cell senescence by regulating ferroptosis

We constructed a UVA-induced photoaging model using mouse skin fibroblasts and treated the cells with the ferroptosis inhibitor FER-1. Compared to the NC group, the UVA group showed decreased skin fibroblast viability, an increased number of senescent cells, elevated iron and ROS levels, and reduced GSH levels. Treatment with FER-1 reversed these effects by increasing skin fibroblast viability, inhibiting cell senescence, reducing iron and ROS levels, and elevating GSH levels (Fig. 2A, B, C, D, and E). Furthermore, compared to the NC group, the UVA group exhibited elevated NRF2 expression and suppressed GPX4 and SLC7A11 expression. This increase in NRF2 may reflect a compensatory cellular response to UVA-induced oxidative stress. FER-1 treatment inhibited NRF2 expression while promoting GPX4 and SLC7A11 expression (Fig. 2F). These findings suggest that UVA induces cell senescence partly through oxidative stress-related ferroptosis, in which NRF2 is activated as part of the endogenous defense mechanism.

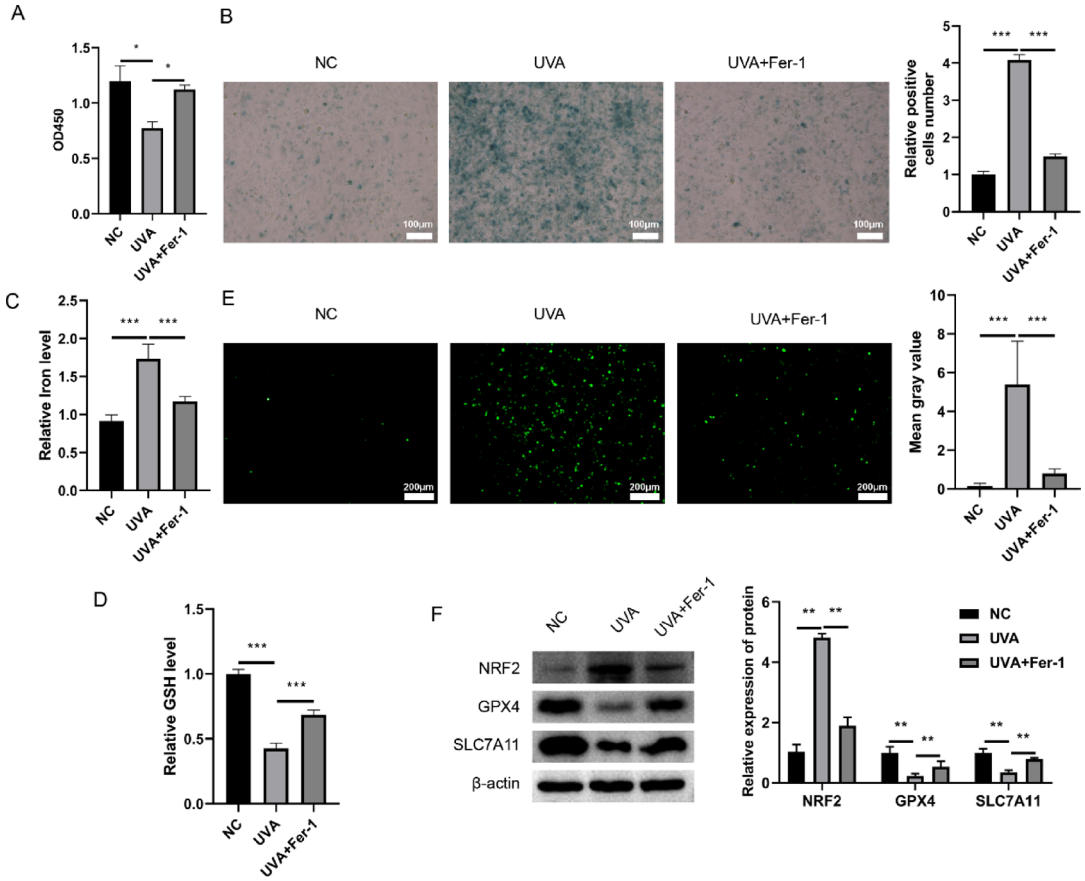

Fig. 2. UVA promoted cell senescence by regulating ferroptosis. (**A**) CCK-8 assay results showed the viability of mouse skin fibroblasts 48 h after treatment. Groups: NC (normal fibroblasts), UVA (6 J/m^2 UVA irradiation), and UVA + Fer-1 (2 μM ferrostatin-1 with 6 J/m^2 UVA). (**B**) SA-β-Gal staining of mouse skin fibroblasts senescence, scale bar = 100 μm. (**C**, **D**, and **E**) Biochemical detection of Iron, GSH, and ROS levels, scale bar = 200 μm. F. Western blot analysis of ferroptosis-related pathway proteins NRF2, GPX4, and SLC7A11, and relative expression levels were quantified based on band intensity normalized to β-actin. $^*P < 0.05$, $^{**}P < 0.01$, $^{***}P < 0.001$.

DPC-CM repaired UVA-induced cell senescence

To evaluate the effects of DPC-CM on UVA-induced cell senescence, mouse skin fibroblasts were first treated with UVA and then with DPC-CM at different concentrations. Compared with the NC group, the viability of skin fibroblasts decreased, and the number of senescent cells increased in the UVA group. However, treatment with low- and high-concentration DPC-CM, as well as RA, improved cell viability and reduced the number of senescent cells (Fig. 3A and B). These findings indicate that DPC-CM effectively repaired UVA-induced cell senescence.

DPC-CM inhibited ferroptosis to regulate UVA-induced cell senescence

Iron and ROS levels were elevated, while GSH levels were reduced in skin fibroblasts in the UVA group compared with the NC group. Treatment with low and high concentrations of DPC-CM decreased iron and ROS levels and increased GSH levels (Fig. 4 A, B and C). Furthermore, compared to the NC group, NRF2 expression was upregulated, and GPX4 and SLC7A11 expressions were downregulated in the UVA group. The observed NRF2 upregulation may represent an adaptive antioxidant response to UVA-induced stress. Treatment with low and high concentrations of DPC-CM reduced NRF2 expression and increased GPX4 and SLC7A11 expressions (Fig. 4D). Additionally, the migration ability of skin fibroblasts in the UVA group was reduced compared with the NC group, whereas treatment with low and high concentrations of DPC-CM improved the migration ability of skin fibroblasts (Fig. 4E). These findings demonstrate that DPC-CM inhibits ferroptosis to regulate UVA-induced cell senescence.

Proteomic characterization of DP cells and DPC-CM and their correlation with ferroptosis regulation

Mass spectrometry was used to examine the association of proteins in mouse DP cells and DPC-CM with ferroptosis regulation. A Venn diagram revealed that 2,996 proteins were identified in DP cells, 198 proteins were identified in DPC-CM, and 99 proteins were common to both (Fig. 5A). GO analysis indicated that these

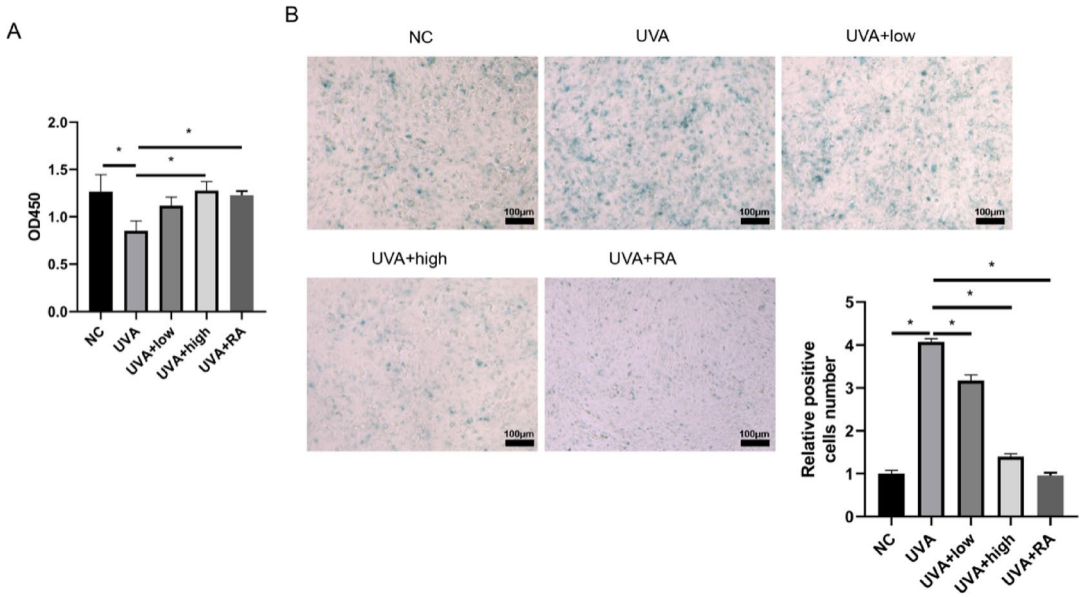

Fig. 3. DPC-CM repaired UVA-induced cell senescence. (**A**) CCK-8 assay determination of the viability of mouse skin fibroblasts. (**B**) SA-β-Gal staining of mouse skin fibroblasts senescence, scale bar = 100 μm. $^{*}P < 0.05$.

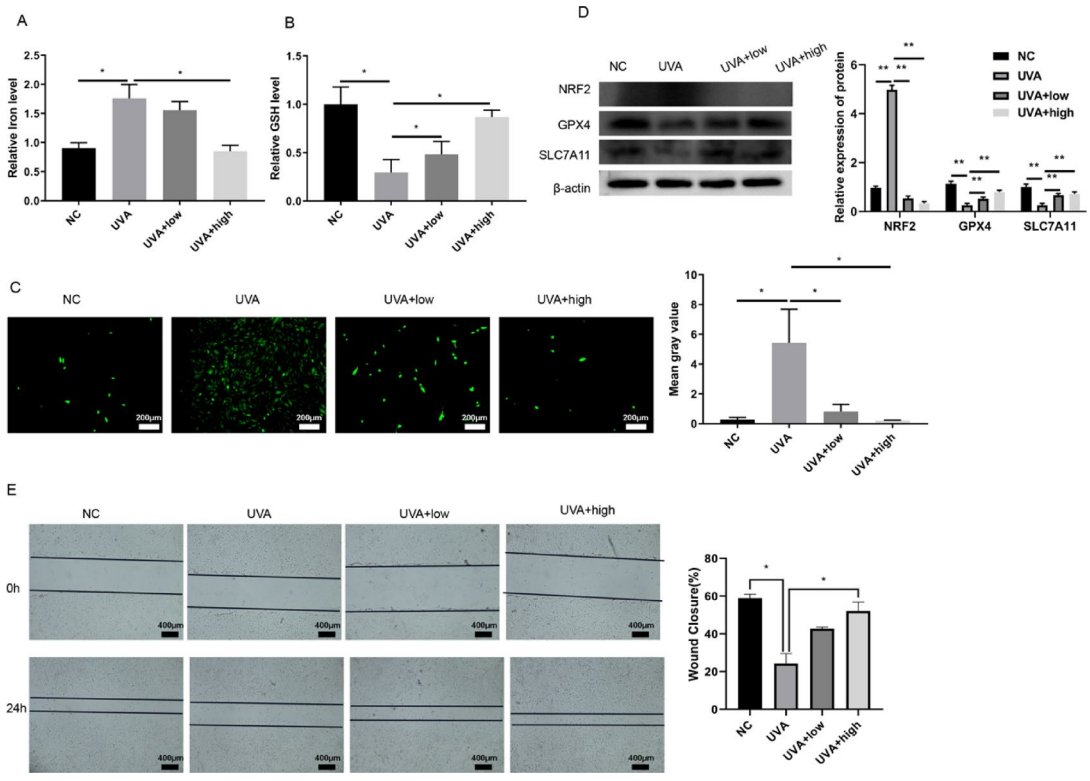

Fig. 4. DPC-CM inhibited ferroptosis to regulate UVA-induced cell senescence. (**A**, **B**, and **C**). Biochemical detection of Iron, GSH, and ROS levels, scale bar = 200 μm. (**D**) Western blot analysis of ferroptosis-related pathway proteins NRF2, GPX4, and SLC7A11, and protein levels were quantified by densitometry, with expression normalized to β-actin. E. Scratch assay assessment of cell migration, scale bar = 400 μm. $^{*}P < 0.05$, $^{**}P < 0.01$.

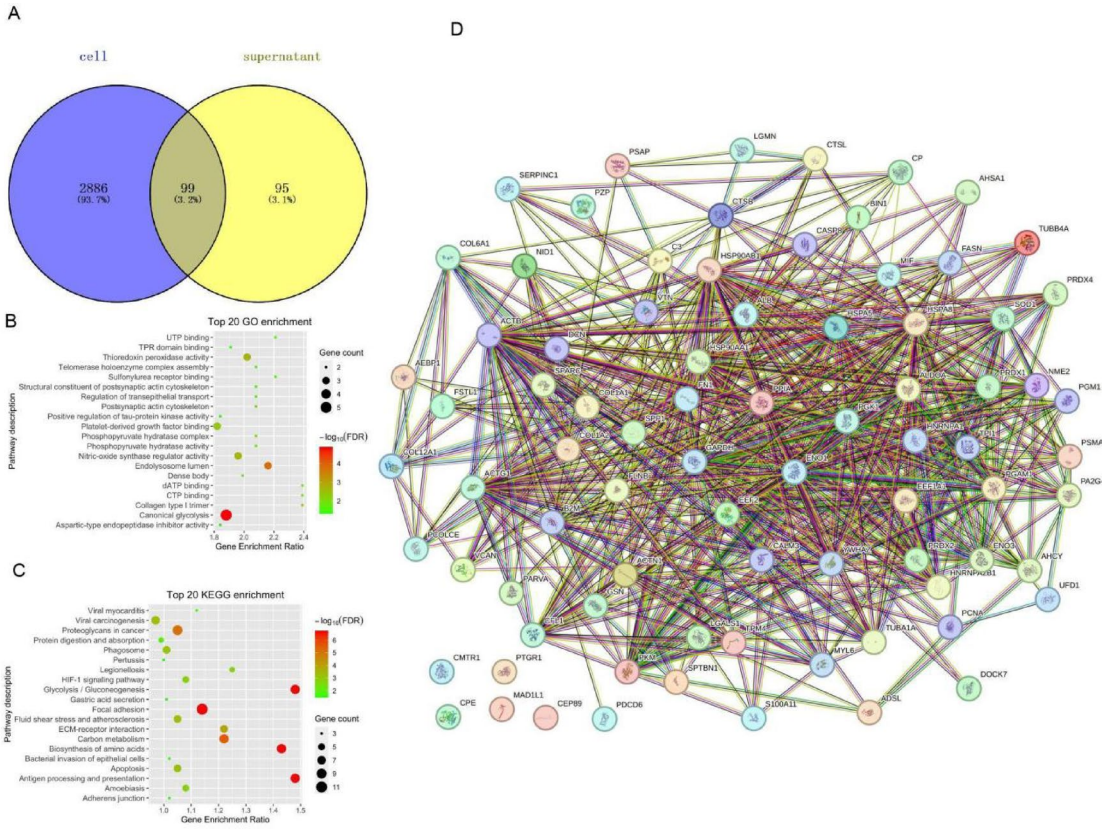

Fig. 5. Mass spectrometry detection of the correlation between proteins and ferroptosis in DP cells and DPC-CM. (**A**) Venn diagram showed that 2996 proteins were identified in DP cells, 198 proteins were identified in DPC-CM, and 99 of these proteins were common to both. (**B**) GO analysis of common proteins. (**C**) KEGG analysis of common proteins. (**D**) PPI analysis of common proteins.

common proteins were primarily enriched in pathways such as canonical glycolysis, platelet-derived growth factor binding, thioredoxin peroxidase activity, nitric oxide synthase regulator activity, and the endolysosome lumen (Fig. 5B). KEGG analysis showed enrichment in pathways including focal adhesion, proteoglycans in cancer, viral carcinogenesis, glycolysis/gluconeogenesis, carbon metabolism, biosynthesis of amino acids, and antigen processing and presentation (Fig. 5C). The PPI network, illustrated in Fig. 5D, highlighted interactions among proteins such as peptidylprolyl isomerase A (PPIA), enolase 1 (ENO1), phosphoglycerate kinase 1 (PGK1), and eukaryotic translation elongation factor 2 (EEF2).

DPC-CM inhibited UVA-induced skin aging in vivo

To determine whether DPC-CM inhibits UVA-induced skin aging in vivo, we assessed the back skin of mice. In the NC group, the back skin appeared red, shiny, elastic, and devoid of wrinkles and visible texture. In the UVA group, the back skin was dark red, rough, and loose, with obvious wrinkles and coarse texture. Treatment with DPC-CM (UVA + CM group) or retinoic acid (UVA + RA group) significantly reduced skin wrinkles, laxity, and dryness (Fig. 6A). H&E staining revealed that, compared to the NC group, the epidermis in the UVA group was significantly thicker with uneven cell arrangement, notable hyperkeratosis, increased incidence of epidermal hyperkeratosis, substantial dermal inflammatory infiltration, and fragmented collagen fibers. In the UVA + CM and UVA + RA groups, the epidermis was notably thinner, structural irregularities were improved, dermal fiber organization was more orderly, and inflammatory infiltration was significantly reduced (Fig. 6B). Masson staining showed that dermal collagen fibers were dense and orderly with normal morphology in the NC group. In contrast, collagen fibers in the UVA group were sparse, disordered, and exhibited reduced spatial density. Treatment with DPC-CM or retinoic acid increased collagen density and restored fiber alignment (Fig. 6C). Additionally, β-Gal activity was elevated, and expressions of Collagen I and α-SMA were reduced in the UVA group compared with the NC group. Treatment with DPC-CM or retinoic acid reduced β-Gal activity and increased Collagen I and α-SMA expressions (Fig. 6D and E). These results indicate that DPC-CM inhibits UVA-induced skin aging in vivo. To exclude potential non-specific effects of the vehicle or passive healing, we also conducted an experiment including PEG alone and PEG + DPC-CM treatment without UVA exposure. During the 7-day observation period, no visible changes were observed in the dorsal skin of either group (Supplementary Fig. 1). This suggests that the therapeutic effects observed in the UVA-induced model are specific to DPC-CM action under oxidative stress. And PEG was employed as the vehicle due to its recognized safety profile, excellent

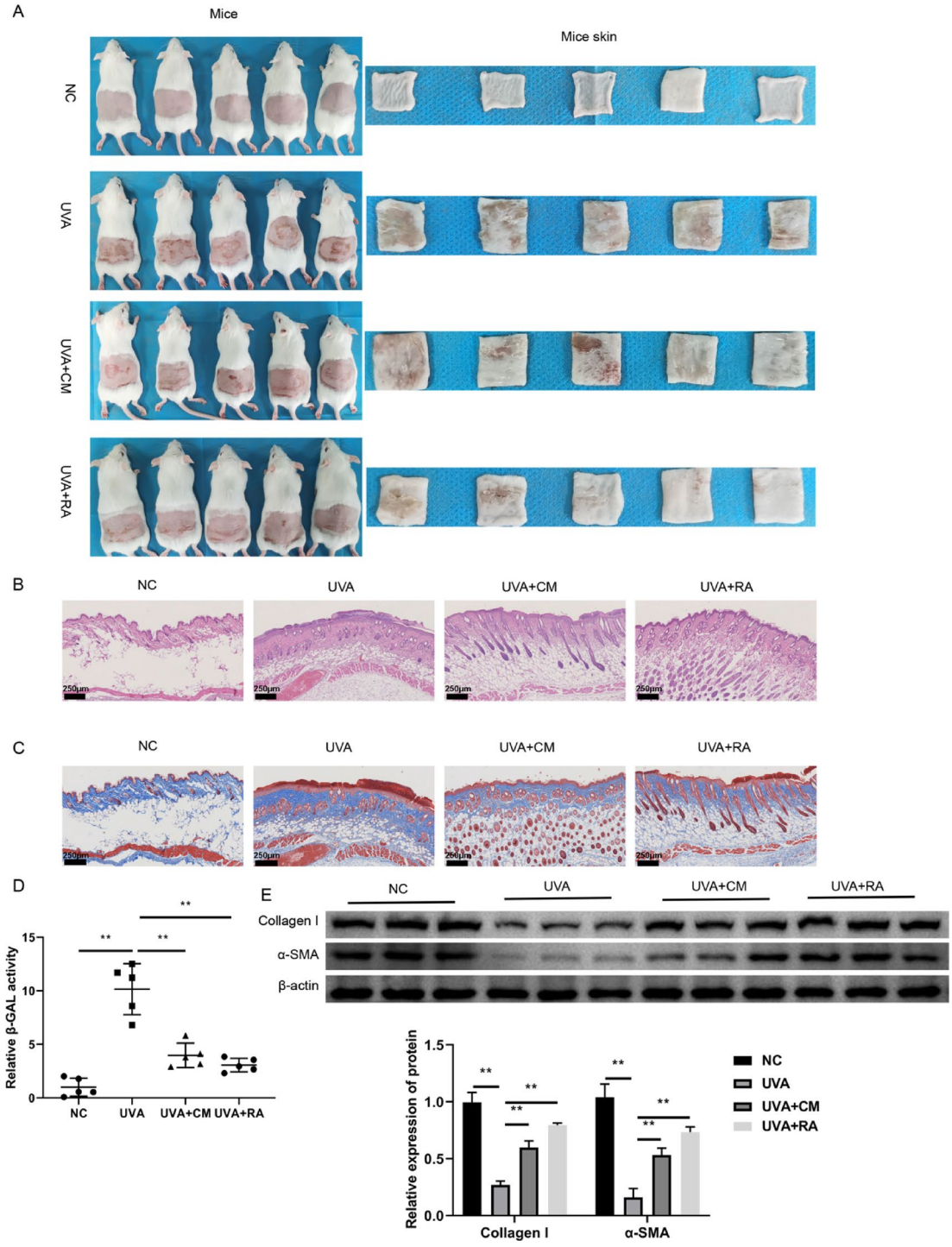

Fig. 6. DPC-CM inhibited UVA-induced skin aging in vivo. (**A**) The morphological changes of the skin surface after modeling (left: mice with skin)/(right: cut skin). (**B**) and (**C**) H&E and Masson staining of the pathological changes of epidermis and dermis, scale bar = 250 μm. (**D**) Detection of β-Gal activity. (**E**). Western blot analysis of Collagen I and α-SMA expressions, and densitometric analysis was performed using β-actin as the internal control. $^{**}P < 0.01$.

biocompatibility, and frequent application in dermatological formulations. Previous studies have demonstrated that topical use of PEG induces negligible skin irritation and is well tolerated in vivo[29,30].

DPC-CM inhibited ferroptosis to regulate UVA-induced skin aging in vivo

Finally, we investigated whether DPC-CM regulates UVA-induced skin aging by inhibiting ferroptosis in vivo. Compared to the NC group, iron and ROS levels were elevated, and GSH levels were reduced in the skin of

mice in the UVA group. Treatment with DPC-CM reduced iron and ROS levels and increased GSH levels in the skin (Fig. 7A, B and C). Moreover, NRF2 expression was upregulated, and GPX4 and SLC7A11 expressions were downregulated in the UVA group compared to the NC group. The upregulation of NRF2 is likely a stress-adaptive response to UVA exposure. Treatment with DPC-CM decreased NRF2 expression while increasing GPX4 and SLC7A11 expressions (Fig. 7D). These results imply that DPC-CM mitigates ferroptosis and oxidative damage, contributing to reduced NRF2 activation.

Taken together, our findings demonstrate that DPC-CM can alleviate UVA-induced oxidative damage and cell senescence by modulating ferroptosis-related pathways. In vitro, DPC-CM treatment enhanced fibroblast viability, reduced intracellular ROS and iron levels, restored GSH content, and upregulated GPX4 and SLC7A11 expression. These changes were accompanied by a decrease in senescence-associated β-galactosidase activity and an improvement in fibroblast migration. In vivo, DPC-CM improved skin texture, reduced epidermal thickening and collagen degradation, and restored the expression of Collagen I and α-SMA. Mass spectrometry analysis identified overlapping proteins between DP cells and DPC-CM, such as PPIA, ENO1, PGK1, and EEF2, which may play roles in the observed effects. A visual summary of these results is provided in Fig. 8.

Discussion

Skin photoaging is caused by changes in the dermal matrix resulting from impaired fibroblast function due to cumulative UVA exposure[31]. The concept of "reduce-improve-protection" is crucial for preventing UV-induced diseases and minimizing damage to human skin[12]. In this study, we explored the role of DP cells in UVA-induced photoaging and their regulatory mechanisms. Our findings demonstrated that DPC-CM effectively inhibited UVA-induced cell and skin aging by suppressing ferroptosis in both in vivo and in vitro models. The role of DP cells and ferroptosis in photoaging has not been reported before, representing the innovative aspect of this study.

Photoaging is a significant exogenous aging factor, leading to morphological and functional decline of the skin. It is strongly influenced by environmental factors, with UV radiation being a primary contributor to skin aging[32]. UV radiation has profound effects on the dermal connective tissue of human skin[33], inducing DNA damage, oxidative stress, and cellular aging[25]. Among UV rays, UVA is the dominant contributor to solar-induced skin aging[34], primarily by causing oxidative stress and promoting degradation of collagen and other matrix components[35]. Repeated UVA exposure disrupts the redox balance and leads to progressive structural changes in the dermis[36]. In 3D cultures under UVA irradiation, fibroblasts acquire an elongated shape, lose dynamic interactions with collagen fibers, and show reduced expression of integrin α2 and α-SMA[31]. Repeated UVA irradiation induces functional decline, which is a key feature of UVA-induced photoaging, making it a suitable in vitro model for study[37]. In this study, mouse skin fibroblasts were treated with UVA to establish a cell photoaging model.

Ferroptosis, an iron-dependent form of regulated cell death[38], is characterized by severe lipid peroxidation and ROS accumulation due to iron overload[39]. This process is driven by the inactivation of GPX4, a key regulatory enzyme, which results from GSH depletion[40]. GSH, a critical component of the cellular antioxidant system[41], plays a central role in reducing ROS through its REDOX capacity. Elevated GSH expression can

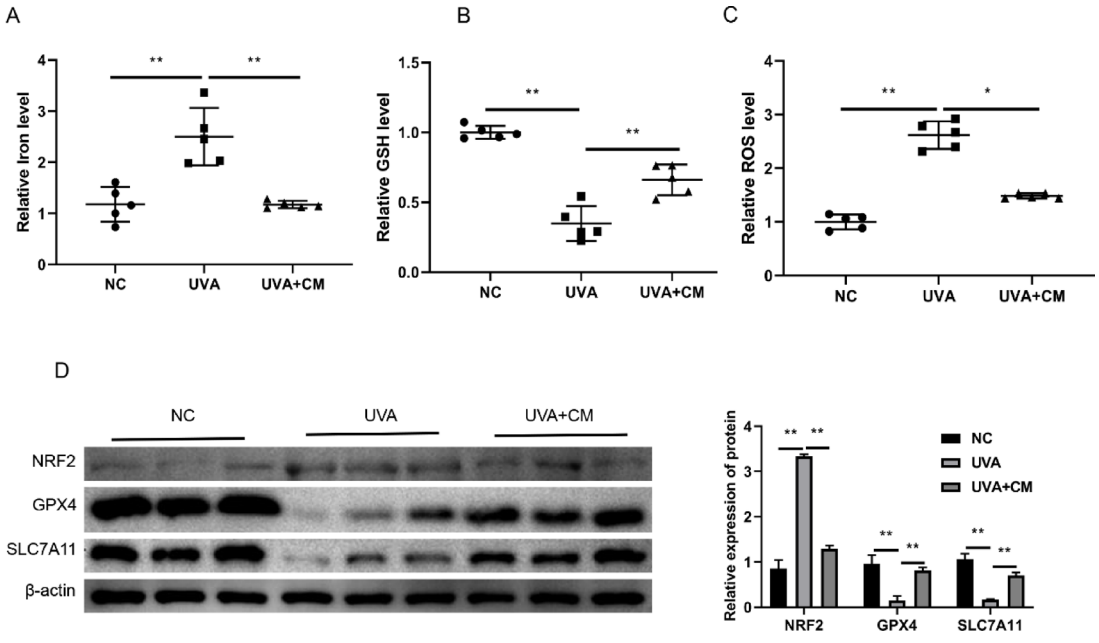

Fig. 7. DPC-CM inhibited ferroptosis to regulate UVA-induced skin aging in vivo. (**A**, **B**, and **C**). Biochemical detection of Iron, GSH, and ROS levels in tissues. D. Western blot analysis of ferroptosis-related pathway proteins NRF2, GPX4, and SLC7A11, and the expression was quantified from Western blot images, and values were normalized to β-actin. $^{*}P<0.05$, $^{**}P<0.01$.

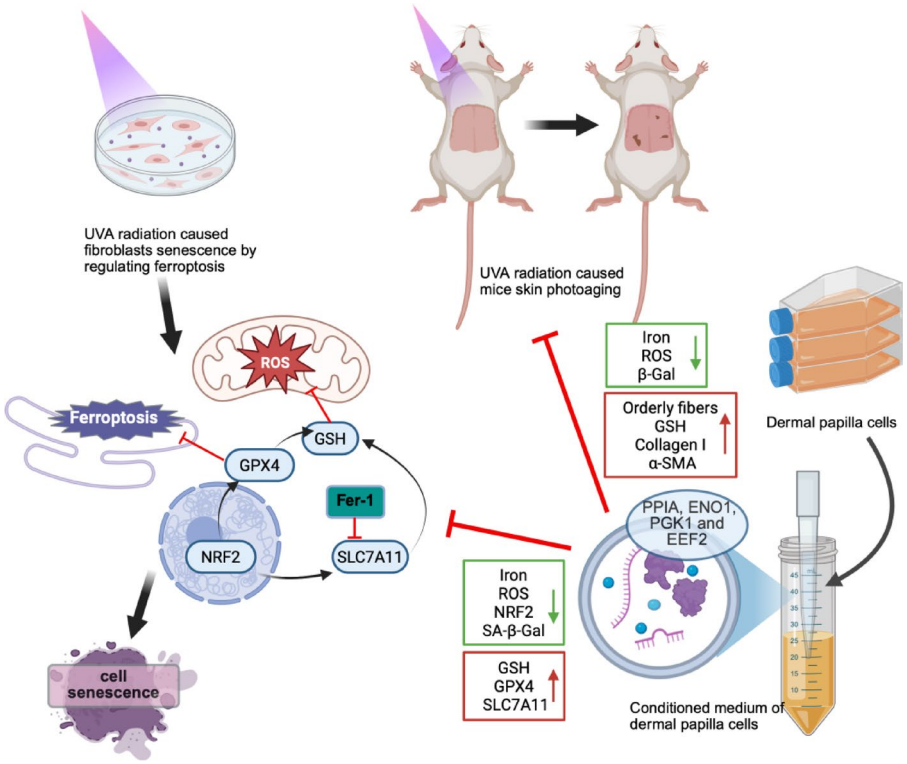

Fig. 8. Schematic diagram illustrating how DPC-CM protects against UVA-induced photoaging. DPC-CM treatment improved antioxidant levels, reduced iron and ROS accumulation, and alleviated signs of cellular senescence in vitro and in vivo. Created in BioRender. Ru, Z. (2025) https://BioRender.com/cx87uig.

inhibit ferroptosis[42]. NRF2 is widely recognized as a master regulator of oxidative stress resistance, primarily by upregulating SLC7A11[43], which facilitates cystine uptake and supports intracellular GSH synthesis. This pathway helps prevent oxidative damage and lipid peroxidation via the GSH-GPX4 axis[44]. A study has shown that circUBE2I overexpression in keratinocytes induces ferroptosis under UVA conditions, an effect that can be prevented by FER-1[45]. In our study, UVA treatment significantly reduced the viability of mouse skin fibroblasts, increased the number of senescent cells, elevated both iron and ROS levels, and decreased GSH levels. We also observed an increase in NRF2 expression, which reflects a compensatory response to oxidative stress[46]. Meanwhile, GPX4 and SLC7A11 were downregulated. FER-1 treatment reversed these changes, including a reduction in NRF2 expression, which indicates that the oxidative burden was alleviated upon inhibition of ferroptosis. These findings suggest that UVA promotes cell senescence, at least in part, through ferroptosis.

Although direct evidence regarding the anti-photoaging effects of other stem cell-derived conditioned media remains limited, available studies have shown that conditioned media from sources such as adipose-derived stem cells (ADSCs) and bone marrow-derived stem cells (BMSCs) possess properties favorable for skin repair. ADSC-CM has been found to improve skin moisture retention, stimulate collagen synthesis, and reduce oxidative stress in damaged skin, indicating a potential role in mitigating photoaging-related changes[47]. Likewise, BMSC-CM has demonstrated efficacy in promoting wound healing and regulating inflammatory responses in UV-damaged skin models[48]. In comparison, DPC-CM may provide distinct advantages. Given the essential role of dermal papilla cells in hair follicle signaling and extracellular matrix regulation, their secretions are likely to exert more direct and pronounced effects on tissue regeneration[49]. Notably, our study uniquely demonstrates that DPC-CM modulates ferroptosis, a regulated cell death pathway linked to oxidative damage and cellular aging-a mechanism not previously reported in other types of stem cell-derived CM. This may contribute to its enhanced efficacy in preventing the persistent structural damage observed in UVA-induced photoaging.

Mass spectrometry analysis identified key proteins associated with the regulation of ferroptosis, including PPIA, ENO1, PGK1, and EEF2. These proteins play critical roles in essential cellular functions that contribute to ferroptosis under conditions of oxidative stress. PPI is an enzyme crucial for protein folding and stabilization, aiding in the maintenance of cellular functions during stress. It may also regulate cellular stress responses, including those initiated by ferroptosis[50]. ENO1 is a key enzyme in glycolysis that generates ATP and is central to energy metabolism[51]. PGK1, another glycolytic enzyme, also contributes to energy production and affects cell survival under stress[52]. The metabolic changes driven by oxidative stress are vital in ferroptosis[53]. Therefore, ENO1 and PGK1 may play a role in modulating ferroptosis by regulating energy levels during oxidative stress. EEF2 plays a crucial role in protein translation[54]. Under stress conditions like ferroptosis, EEF2 may contribute to the disruption of protein synthesis by inhibiting translation in response to oxidative stress. However, it should be noted that the functional relevance of these proteins was inferred from proteomic associations, and

direct validation through gene silencing or inhibition assays was not performed in this study. This remains an important limitation and a key focus for future investigation.

Continuous exposure to solar UV radiation can lead to photoaging and photocarcinogenesis, compromising the skin's barrier function by altering cellular and structural components[23]. Stem cells play a critical role in tissue development, rejuvenation, and regeneration, governed by specialized local microenvironments or "niches"[55]. DP cells, as key regulatory entities in hair follicles, promote hair formation and growth through interactions with epithelial cells[56]. The transition of hair follicles from resting to growth phases, essential for regulating hair growth, is largely dependent on the activation of DP cells[57]. Hair follicle DP cells are specialized mesenchymal cells that play a vital role in the formation, growth, and cycling of hair. They are considered a promising cell source in hair regenerative medicine[58]. DP cells can regenerate new hair follicles and induce hair growth, providing potential therapeutic strategies for hair loss treatment[59]. UVA exposure has been reported to induce hair follicle photoaging by reducing hair follicle-associated stem cells, leading to hair follicle miniaturization and hair graying[60]. However, the specific functions of DPC-CM and their connection to ferroptosis in photoaging remain unclear.

Our study revealed that DPC-CM mitigates UVA-induced cell and skin aging in both in vivo and in vitro settings. Moreover, we demonstrated that DPC-CM suppresses ferroptosis, thereby attenuating the aging process triggered by UVA exposure. Nevertheless, this work has several limitations, as it represents an initial step in exploring this mechanism. A key limitation lies in the use of a murine model, which, while informative, does not fully replicate the complexity of human skin architecture and physiology. In addition, despite efforts to minimize inconsistencies, variability between DPC-CM batches remains a concern and may affect the reproducibility of results. The precise molecular mechanisms through which DPC-CM modulates ferroptosis also remain to be clarified, especially in relation to its translational potential. Future studies aimed at addressing these aspects will be essential for confirming and expanding upon our current findings.

Given its capacity to suppress ferroptosis and alleviate UVA-induced skin aging, DPC-CM emerges as a promising therapeutic option for anti-photoaging treatment. Nonetheless, translating these preclinical findings into practical clinical applications involves several foreseeable hurdles, including maintaining batch-to-batch consistency, establishing standardized manufacturing protocols, and verifying long-term safety and effectiveness in human subjects. In our study, only DPC at passages 3 to 6 (P3-P6) were collected to ensure cellular quality and consistency. Besides, practical factors such as formulation stability, optimal storage conditions (e.g., temperature, lyophilization), and delivery strategies (e.g., topical creams, hydrogels, or microneedle systems) will require systematic evaluation to facilitate clinical translation. Regulatory considerations related to cell-derived products, including quality control and reproducibility, must also be addressed in future research. Continued research is warranted to resolve these challenges and to explore the viability of formulating DPC-CM-based products for dermatological use.

In conclusion, this study presents, for the first time, a mechanism involving DP cells and ferroptosis in the context of photoaging. Our results demonstrate that DPC-CM inhibits UVA-induced cell and skin aging by suppressing ferroptosis in vivo and in vitro. Understanding the role of ferroptosis in photoaging and intervening in its pathological progression may provide novel insights for clinical strategies aimed at effectively managing photoaging.

Data availability

The data generated in the present study are included in the figures of this article.

Received: 31 January 2025; Accepted: 24 June 2025
Published online: 09 July 2025

References

1. Bai, G. L. et al. Rapamycin protects skin fibroblasts from UVA-Induced photoaging by inhibition of p53 and phosphorylated HSP27. *Front. Cell. Dev Biol.* **9**, 633331. https://doi.org/10.3389/fcell.2021.633331 (2021).
2. Battie, C. et al. New insights in photoaging, UVA induced damage and skin types. *Exp. Dermatol.* **23**(Suppl 1), 7–12. https://doi.org/10.1111/exd.12388 (2014).
3. Zhang, Y. et al. Circ_0011129 encapsulated by the small extracellular vesicles derived from human stem cells ameliorate skin photoaging. *Int. J. Mol. Sci.* **23**, 15390. https://doi.org/10.3390/ijms232315390 (2022).
4. Chu, M. et al. Disulfiram/copper induce ferroptosis in triple-negative breast cancer cell line MDA-MB-231. *Front. Biosci. (Landmark Ed)* **28**, 186. https://doi.org/10.31083/j.fbl2808186 (2023).
5. Xiong, D., Hu, W., Han, X. & Cai, Y. Rhein inhibited ferroptosis and EMT to attenuate diabetic nephropathy by regulating the Rac1/NOX1/β-catenin axis. *Front. Biosci. (Landmark Ed)* **28**, 100. https://doi.org/10.31083/j.fbl2805100 (2023).
6. Gu, X. et al. METTL14-mediated m6A modification of TUG1 represses ferroptosis in alzheimer's disease via inhibiting GDF15 ubiquitination. *Front. Biosci. (Landmark Ed)* **29**, 298. https://doi.org/10.31083/j.fbl2908298 (2024).
7. Huang, M., Wang, Y., Wu, X. & Li, W. Crosstalk between endoplasmic reticulum stress and ferroptosis in liver diseases. *Front. Biosci. (Landmark Ed)* **29**, 221. https://doi.org/10.31083/j.fbl2906221 (2024).
8. Chen, X., Li, J., Kang, R., Klionsky, D. J. & Tang, D. Ferroptosis: Machinery and regulation. *Autophagy* **17**, 2054–2081. https://doi.org/10.1080/15548627.2020.1810918 (2021).
9. Li, J. et al. Ferroptosis: Past, present and future. *Cell Death Dis.* **11**, 88. https://doi.org/10.1038/s41419-020-2298-2 (2020).
10. Zhang, P. C. et al. Variation of ferroptosis-related markers in HaCaT cell photoaging models induced by UVB. *Clin. Cosmet. Investig. Dermatol.* **16**, 3147–3155. https://doi.org/10.2147/ccid.S433071 (2023).
11. Sun, J. et al. Selenomethionine in gelatin methacryloyl hydrogels: Modulating ferroptosis to attenuate skin aging. *Bioact. Mate.r* **35**, 495–516. https://doi.org/10.1016/j.bioactmat.2024.02.013 (2024).
12. Termer, M. et al. Methoxy-monobenzoylmethane protects skin from UV-induced damages in a randomized, placebo controlled, double-blinded human in vivo study and prevents signs of inflammation while improving the skin barrier. *Dermatol. Ther. (Heidelb)* **12**, 435–449. https://doi.org/10.1007/s13555-021-00652-3 (2022).

13. Khandpur, S., Gupta, S. & Gunaabalaji, D. R. Stem cell therapy in dermatology. *Indian J. Dermatol. Venereol. Leprol.* **87**, 753–767. https://doi.org/10.25259/ijdvl_19_20 (2021).
14. Li, K. J. et al. Recent advances in exosomal non-coding RNA-based therapeutic approaches for photoaging. *Skin Res. Technol.* **29**, e13463. https://doi.org/10.1111/srt.13463 (2023).
15. Jo, H. et al. Applications of mesenchymal stem cells in skin regeneration and rejuvenation. *Int. J. Mol. Sci.* https://doi.org/10.3390/ijms22052410 (2021).
16. Topouzi, H., Logan, N. J., Williams, G. & Higgins, C. A. Methods for the isolation and 3D culture of dermal papilla cells from human hair follicles. *Exp. Dermatol.* **26**, 491–496. https://doi.org/10.1111/exd.13368 (2017).
17. Gan, Y. et al. Ficoll density gradient sedimentation isolation of pelage hair follicle mesenchymal stem cells from adult mouse back skin: A novel method for hair follicle mesenchymal stem cells isolation. *Stem Cell Res. Ther.* **13**, 372. https://doi.org/10.1186/s13287-022-03051-3 (2022).
18. Chen, Y. et al. Sustained release of dermal papilla-derived extracellular vesicles from injectable microgel promotes hair growth. *Theranostics* **10**, 1454–1478. https://doi.org/10.7150/thno.39566 (2020).
19. Luo, X. et al. Isolation, characterization and differentiation of dermal papilla cells from small-tail Han sheep. *Anim. Biotechnol.* **34**, 3475–3482. https://doi.org/10.1080/10495398.2022.2156873 (2023).
20. Oppenheimer, F. M. et al. Dermal papilla cells cultured as spheres improve angiogenesis. *Exp. Dermatol.* **33**, e15038. https://doi.org/10.1111/exd.15038 (2024).
21. Maguire, G. Stem cell therapy without the cells. *Commun. Integr. Biol.* **6**, e26631. https://doi.org/10.4161/cib.26631 (2013).
22. Zou, X. et al. Multi-omics analysis of an in vitro photoaging model and protective effect of umbilical cord mesenchymal stem cell-conditioned medium. *Stem Cell Res. Ther.* **13**, 435. https://doi.org/10.1186/s13287-022-03137-y (2022).
23. Gong, M. et al. ADSCs inhibit photoaging- and photocarcinogenesis-related inflammatory responses and extracellular matrix degradation. *J. Cell Biochem.* **121**, 1205–1215. https://doi.org/10.1002/jcb.29354 (2020).
24. Gunawardena, T. N. A. et al. Dental derived stem cell conditioned media for hair growth stimulation. *PLoS ONE* **14**, e0216003. https://doi.org/10.1371/journal.pone.0216003 (2019).
25. Chen, Q. et al. Metformin attenuates UVA-induced skin photoaging by suppressing mitophagy and the PI3K/AKT/mTOR pathway. *Int. J. Mol. Sci.* **23**, 6960. https://doi.org/10.3390/ijms23136960 (2022).
26. Yoon, S. Y. et al. An important role of cutaneous lymphatic vessels in coordinating and promoting anagen hair follicle growth. *PLoS ONE* **14**, e0220341. https://doi.org/10.1371/journal.pone.0220341 (2019).
27. Kanehisa, M., Sato, Y., Kawashima, M., Furumichi, M. & Tanabe, M. KEGG as a reference resource for gene and protein annotation. *Nucleic Acids Res.* **44**, D457-462. https://doi.org/10.1093/nar/gkv1070 (2016).
28. Kanehisa, M. & Goto, S. KEGG: Kyoto encyclopedia of genes and genomes. *Nucleic Acids Res.* **28**, 27–30. https://doi.org/10.1093/nar/28.1.27 (2000).
29. Patel, V. & Gaurav, V. Role of polyethylene glycol in dermatology. *Indian Dermatol. Online J.* **16**, 227–234. https://doi.org/10.4103/idoj.idoj_648_24 (2025).
30. Sabbieti, M. G. et al. In vivo biocompatibility of p(HPMAm-lac)-PEG hydrogels hybridized with hyaluronan. *J. Tissue Eng. Regen. Med.* **11**, 3056–3067. https://doi.org/10.1002/term.2207 (2017).
31. Nakyai, W. et al. Effects of repeated UVA irradiation on human skin fibroblasts embedded in 3D tense collagen matrix. *Photochem. Photobiol.* **94**, 715–724. https://doi.org/10.1111/php.12895 (2018).
32. Endo, K. et al. Impairment of the autophagy system in repetitively UVA-irradiated fibroblasts. *Photodermatol. Photoimmunol. Photomed.* **36**, 111–117. https://doi.org/10.1111/phpp.12516 (2020).
33. Liu, Y. et al. Photo-aging evaluation - in vitro biological endpoints combined with collagen density assessment with multi-photon microscopy. *J. Dermatol. Sci.* **105**, 37–44. https://doi.org/10.1016/j.jdermsci.2021.12.002 (2022).
34. Lan, C. E., Hung, Y. T., Fang, A. H. & Ching-Shuang, W. Effects of irradiance on UVA-induced skin aging. *J. Dermatol. Sci.* **94**, 220–228. https://doi.org/10.1016/j.jdermsci.2019.03.005 (2019).
35. Fu, H. et al. Anti-photoaging effect of *Rhodiola rosea* fermented by *Lactobacillus plantarum* on UVA-damaged fibroblasts. *Nutrients* **14**, 2324. https://doi.org/10.3390/nu14112324 (2022).
36. Hseu, Y. C. et al. Trans-cinnamic acid attenuates UVA-induced photoaging through inhibition of AP-1 activation and induction of Nrf2-mediated antioxidant genes in human skin fibroblasts. *J. Dermatol. Sci.* **90**, 123–134. https://doi.org/10.1016/j.jdermsci.2018.01.004 (2018).
37. Nakyai, W., Saraphanchotiwitthaya, A., Viennet, C., Humbert, P. & Viyoch, J. An in vitro model for fibroblast photoaging comparing single and repeated UVA irradiations. *Photochem. Photobiol.* **93**, 1462–1471. https://doi.org/10.1111/php.12801 (2017).
38. Chen, Y., Fang, Z. M., Yi, X., Wei, X. & Jiang, D. S. The interaction between ferroptosis and inflammatory signaling pathways. *Cell Death Dis.* **14**, 205. https://doi.org/10.1038/s41419-023-05716-0 (2023).
39. Zhou, H. et al. NCOA4-mediated ferritinophagy is involved in ionizing radiation-induced ferroptosis of intestinal epithelial cells. *Redox Biol.* **55**, 102413. https://doi.org/10.1016/j.redox.2022.102413 (2022).
40. Yang, W. S. & Stockwell, B. R. Ferroptosis: Death by lipid peroxidation. *Trends Cell Biol.* **26**, 165–176. https://doi.org/10.1016/j.tcb.2015.10.014 (2016).
41. Niu, B. et al. Application of glutathione depletion in cancer therapy: Enhanced ROS-based therapy, ferroptosis, and chemotherapy. *Biomaterials* **277**, 121110. https://doi.org/10.1016/j.biomaterials.2021.121110 (2021).
42. Rochette, L. et al. Lipid peroxidation and iron metabolism: Two corner stones in the homeostasis control of ferroptosis. *Int. J. Mol. Sci.* **24**, 449. https://doi.org/10.3390/ijms24010449 (2022).
43. Rosell, R. et al. Biological insights in non-small cell lung cancer. *Cancer Biol. Med.* **20**, 500–518. https://doi.org/10.20892/j.issn.2095-3941.2023.0108 (2023).
44. Mathew, M. et al. Induction of oxidative stress and ferroptosis in triple-negative breast cancer cells by niclosamide via blockade of the function and expression of SLC38A5 and SLC7A11. *Antioxidants (Basel)* **13**, 291. https://doi.org/10.3390/antiox13030291 (2024).
45. Yi, P. et al. A novel UVA-associated circUBE2I mediates ferroptosis in HaCaT cells. *Photochem. Photobiol.* **100**, 1365–1377. https://doi.org/10.1111/php.13885 (2023).
46. Bae, T., Hallis, S. P. & Kwak, M. K. Hypoxia, oxidative stress, and the interplay of HIFs and NRF2 signaling in cancer. *Exp. Mol. Med.* **56**, 501–514. https://doi.org/10.1038/s12276-024-01180-8 (2024).
47. Li, A. N. et al. Regenerative potential nanomedicine of adipocyte stem cell-derived exosomes in senescent skin tissue. *Int. J. Nanomed.* **19**, 13149–13163. https://doi.org/10.2147/ijn.S470225 (2024).
48. Kim, S. N. et al. The effects of human bone marrow-derived mesenchymal stem cell conditioned media produced with fetal bovine serum or human platelet lysate on skin rejuvenation characteristics. *Int. J. Stem Cells* **14**, 94–102. https://doi.org/10.15283/ijsc20070 (2021).
49. Ahmed, M. N. et al. Dental pulp cell sheets enhance facial nerve regeneration via local neurotrophic factor delivery. *Tissue Eng. Part A* **27**, 1128–1139. https://doi.org/10.1089/ten.TEA.2020.0265 (2021).
50. Keleş, E. et al. Phthalate exposure induces cell death and ferroptosis in neonatal microglial cells. *Turk. J. Med. Sci.* **54**, 1102–1115. https://doi.org/10.55730/1300-0144.5889 (2024).
51. Zhang, G., Zhao, X. & Liu, W. NEDD4L inhibits glycolysis and proliferation of cancer cells in oral squamous cell carcinoma by inducing ENO1 ubiquitination and degradation. *Cancer Biol. Ther.* **23**, 243–253. https://doi.org/10.1080/15384047.2022.2054244 (2022).

52. Lu, J. et al. Energy metabolism is co-determined by genetic variants in chronic lymphocytic leukemia and influences drug sensitivity. *Haematologica* **104**, 1830–1840. https://doi.org/10.3324/haematol.2018.203067 (2019).
53. Park, M. W. et al. NOX4 promotes ferroptosis of astrocytes by oxidative stress-induced lipid peroxidation via the impairment of mitochondrial metabolism in Alzheimer's diseases. *Redox Biol.* **41**, 101947. https://doi.org/10.1016/j.redox.2021.101947 (2021).
54. Francis, J. W. et al. FAM86A methylation of eEF2 links mRNA translation elongation to tumorigenesis. *Mol. Cell* **84**, 1753-1763. e1757. https://doi.org/10.1016/j.molcel.2024.02.037 (2024).
55. Clevers, H., Loh, K. M. & Nusse, R. Stem cell signalling. An integral program for tissue renewal and regeneration: Wnt signaling and stem cell control. *Science* **346**, 1248012. https://doi.org/10.1126/science.1248012 (2014).
56. Abreu, C. M. et al. Rescuing key native traits in cultured dermal papilla cells for human hair regeneration. *J. Adv. Res.* **30**, 103–112. https://doi.org/10.1016/j.jare.2020.10.006 (2021).
57. Kim, H. et al. Potential of colostrum-derived exosomes for promoting hair regeneration through the transition from telogen to anagen phase. *Front. Cell. Dev. Biol.* **10**, 815205. https://doi.org/10.3389/fcell.2022.815205 (2022).
58. Yan, L. et al. Electrical stimulation to human dermal papilla cells for hair regenerative medicine. *J. Biosci. Bioeng.* **133**, 281–290. https://doi.org/10.1016/j.jbiosc.2021.12.003 (2022).
59. Gao, L. et al. Large-scale isolation of functional dermal papilla cells using novel surface marker LEPTIN Receptor. *Cytometry A* **101**, 675–681. https://doi.org/10.1002/cyto.a.24569 (2022).
60. Zhai, X., Gong, M., Peng, Y. & Yang, D. Effects of UV induced-photoaging on the hair follicle cycle of C57BL6/J mice. *Clin. Cosmet. Investig. Dermatol.* **14**, 527–539. https://doi.org/10.2147/ccid.S310487 (2021).

Acknowledgements
Not applicable.

Author contributions
Conceptualization, Methodology, Validation: Z.R., L.Z., and Z.H. Formal analysis, Investigation, Visualization: Y.W., Q.Q., Y.M. Writing—Original Draft: Z.R. Data Curation, Writing—Review & Editing: Z.R., Y.W., Q.Q., Y.M., L.Z., and Z.H..

Funding
This work was supported by National Natural Science Foundation of China (Grant number 82172235).

Declarations

Competing interests
The authors declare no competing interests.

Ethical approval
All animal experiments were authorized by Guangzhou Forevergen Medical Laboratory Animal Center committee (approval number IACUC-AEWC-F231112027). Moreover, animal studies were performed in accordance with ARRIVE guidelines and the IACUC Handbook (third edition).

Additional information
Supplementary Information The online version contains supplementary material available at https://doi.org/10.1038/s41598-025-08968-2.

Correspondence and requests for materials should be addressed to L.Z. or Z.H.